IL NUOVO CIMENTO Vol. 26 C, N. 5 Settembre-Ottobre 2003
DOI 10.1393/ncc/i2003-10008-6

Test of high-energy hadronic interaction models with high-altitude cosmic-ray data(*)

A. Haungs(1)(**) and J. Kempa(2)

(1) *Institut für Kernphysik, Forschungszentrum Karlsruhe - D-76021 Karlsruhe, Germany*
(2) *Warsaw University of Technology, Off-Campus Plock - Lukasiewicza 17 PL-09400 Plock, Poland*

(ricevuto il 23 Gennaio 2003; revisionato il 18 Agosto 2003; approvato l'8 Settembre 2003)

Summary. — Emulsion experiments placed at high mountain altitudes register hadrons and high-energy γ-rays with an energy threshold in the TeV region. These secondary shower particles are produced in the forward direction of interactions of mainly primary protons and alpha-particles in the Earth's atmosphere. Single γ's and hadrons are mainly produced by the interactions of the primary cosmic-ray nuclei of primary energy below 10^{15} eV. Therefore the measurements are sensitive to the physics of high-energy hadronic interaction models, *e.g.*, as implemented in the Monte Carlo air shower simulation program CORSIKA. By use of detailed simulations invoking various different models for the hadronic interactions we compare the predictions for the single-particle spectra with data of the Pamir experiment. For higher primary energies characteristics of so-called gamma-ray families are used for the comparisons. Including detailed simulations for the Pamir detector we found that the data are incompatible with the HDPM and SIBYLL 1.6 models, but are in agreement with QGSJET, neXus, and VENUS.

PACS 96.40.De – Composition, energy spectra, and interactions.
PACS 98.70.Sa – Cosmic rays (including sources, origin, acceleration, and interactions).

1. – Introduction

Monte Carlo simulations of extensive air showers are widely used for the reconstruction and interpretation of indirect cosmic-ray measurements. They are based on various high-energy interaction models currently under debate. The validity of these models is a problem increasing with the improved precision of the measurements by experiments like KASCADE [1,2], where a large set of observables is reconstructed for single showers.

(*) The authors of this paper have agreed to not receive the proofs for correction.
(**) E-mail: haungs@ik.fzk.de

Their experimental results turn out to be sensitive to the specific features of the theoretical approaches for the interaction of high-energy protons or nuclei with air-nuclei. Unfortunately, the *a priori* unknown elemental composition and primary energy spectrum in the PeV region obscures the information of the data in view of the hadronic interaction. Vice versa unknown interaction features prevent to deduce definite conclusions about the main goals of EAS experiments determining composition and energy spectrum of the PeV cosmic rays.

Experiments at high mountain altitudes at Pamir (4370 m a.s.l.) or Mt. Chacaltaya (5200 m a.s.l.) measure electrons, gamma-rays, and hadrons with high-energy thresholds in the TeV region by emulsions or X-ray films (XEC detectors) [3]. The accessible observable in such experiments is the optical density (or darkness) of spots produced in emulsion or X-ray films interspersed between the absorbers, which are typically built by thin lead plates. In addition to the reconstruction of the cores of extensive air-showers by studying so-called particle families, integral measurements of single hadrons and electrons/gamma-rays are performed. At high altitudes these particles stem mainly from primary cosmic rays of energies below 1 PeV and have been produced in extreme forward direction. This explains the special suitability of these measurements for tests of high-energy hadronic interaction models: In the primary energy region of 10–100 TeV the elemental composition and flux of the cosmic rays are approximately known from direct measurements on balloons or satellites. The sensitivity of the emulsion experiments in the extreme forward direction of the interaction carries information complementary to the data of accelerator experiments to which the interaction cross-sections and the particle spectra are adjusted.

In the present paper we study the inclusive flux of e/γ and hadrons for the Pamir experiment predicted by different high-energy interaction models, all embedded in the air-shower simulation program CORSIKA [4]. The predicted flux of the electromagnetic component, taking into account a detailed simulation of the detector response, is compared with the measured distributions of the Pamir experiment. Emphasis is put on the sensitivity for discrimination of the current models en vogue, independently of the accelerator data used for the extrapolation to the terra incognita. The considered observable is the optical density of spots displayed in X-ray films. Additionally some characteristic features of e/γ-families are reconstructed and compared with measurements. For all observables large differences between the various theoretical approaches are revealed. This allows to exclude some current models by comparing with measurements despite their large statistical and systematic uncertainties.

2. – Air-shower simulations

For the following analyses air-shower events are generated using eight different interaction model codes implemented in the air-shower simulation code CORSIKA: VENUS (vers.4.12 [5]), QGSJET (vers. of 1998 [6]), SIBYLL (vers.1.6 [7]), HDPM [4], DPMJET (vers.2.4 [8]), SIBYLL (vers.2.1 [9]), QGSJET (vers. of 2001 [10]), and NEXUS (vers.2.01 [11]). Basically CORSIKA version 5.62 is used except for the last three models which are embedded in CORSIKA version 6.01. All models are adapted in the lower energy range to results from collider experiments, using extrapolations and/or theoretical assumptions to describe the extreme forward direction and the hadronic interactions at higher energies. VENUS, QGSJET, DPMJET, and NEXUS are based on the Gribov-Regge theory which considers multi-pomeron exchange as the relevant process of hadron-nucleon (hadron-nucleus, nucleus-nucleus) scattering. Describing the interac-

tion the algorithms include several main steps: definition of the interaction topology (how many elementary collisions occur, how many pomerons are exchanged in each collision, etc.), energy-momentum sharing between the pomerons, and the formation and hadronization of the strings resulting from the exchanged pomerons. The models mainly differ by their handling of these stages, in particular, by the treatment of the so-called diffraction dissociation mechanism, by the generalization of the Gribov-Regge approach in case of interactions with nuclei, by the parameter choices for the energy-momentum sharing, and by the hadronization algorithm. Additionally, QGSJET, DPMJET, and NEXUS take into account the contribution of semihard processes (perturbative minijet production) which starts to play an important role at PeV energies whereas VENUS and NEXUS account for secondary particle cascading processes. For VENUS the maximum possible energy of the reactions is limited to 20 PeV which is well above the needed range for the present analyses. A special feature of the NEXUS model is the universal approach to high-energy interactions which allow to tune the model parameters on the basis of a consistent treatment of various pomeron-pomeron interactions. The SIBYLL model is based on the minijet philosophy, *i.e.* it assigns the primary energy dependence of the interaction characteristics solely to the increasing production of minijets, whereas the underlying soft interaction is considered to be of scaling type and is described by the production of only a pair of strings connecting valence quarks of the initial hadrons. Finally HDPM is an empirical model inspired by the Gribov-Regge theory where the hadron-hadron interactions are governed by the production of one pair of strings at all energies with relevant parameter values to reproduce accelerator data in cross-section and particle spectra and with extrapolations to higher energies. Both, SIBYLL and HDPM use the superposition prescription to treat nucleus-nucleus collisions. QGSJET 01 differs from the version QGSJET 98 by adjusting the fit to the larger cross-section of reanalyzed collider data and by a modified diffraction dissociation algorithm. The version 2.1 of the SIBYLL model includes multiple pomeron exchanges for the description of soft processes and a corrected diffraction algorithm which moves it closer to the models based on the Gribov-Regge theory. For a more detailed description of the philosophy of the models and their differences see ref. [4] and references therein.

For each model and for three different nuclei (H, He, Fe) 500000 events have been generated, except for the models DPMJET and NEXUS where somewhat fewer events have been simulated in view of the long computing time required for these codes. In the case of primary protons the simulations cover the energy range of 10^{13} eV–10^{16} eV following a power law $\mathrm{d}N/\mathrm{d}E \propto E^{-\gamma}$ with slope $\gamma_{\mathrm{H}} = 2.75$ and isotropic incidence up to 40° zenith distance. In the case of primary helium (iron) the used slope is $\gamma_{\mathrm{He}} = 2.62$ ($\gamma_{\mathrm{Fe}} = 2.60$) in the energy range $2 \cdot 10^{13}$ eV–10^{16} eV (10^{14} eV–10^{16} eV). The slopes were taken from a compilation of direct measurements [12]. All secondary particles with energies larger than 1 TeV at the observation level of the Pamir experiment (4370 m) are taken into account. For the electromagnetic interactions the EGS4 [13] model is used. Parameters of the US standard atmosphere [4] and the magnetic field of the Pamir observation location are included in the present simulations.

Figure 1 compares the energy spectra of hadrons and electromagnetic particles produced by primary protons for all interaction models. While the particle distributions reflect somehow the primary energy slope (differences of the slopes are within statistical uncertainties), the absolute scales of the predictions differ significantly (table I). The SIBYLL 1.6 and HDPM produce obviously more particles and DPMJET and QGSJET 01 a smaller number of particles than the other models. QGSJET 98 and NEXUS give quite similar predictions for both particle types, VENUS agrees with them in the electro-

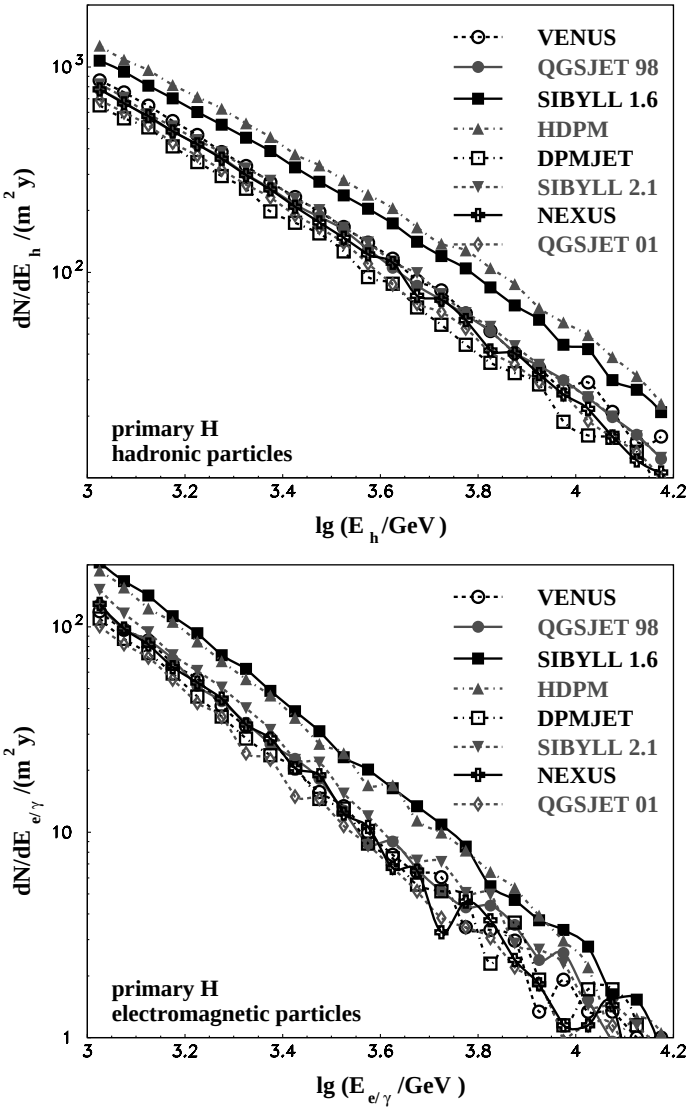

Fig. 1. – The energy spectra of hadronic and electromagnetic shower particles above 1 TeV produced by primary protons as simulated for the Pamir observation level for different interaction models. The statistical uncertainties of the simulations are not plotted, but affect the tail of the spectra. The lines are for guiding the eyes, only.

magnetic part, but produces slightly more hadrons, especially below 3 TeV. SIBYLL 2.1 behaves in the opposite way: It is in agreement with QGSJET 98 and NEXUS for the hadronic part but predicts a higher number of electromagnetic particles. With the fair assumption that the multiplicity of pions, generated by the interaction, is responsible for the ratio of hadrons to electromagnetic particles, not only a sensitivity to the cross-sections, but also to the multiplicity distribution at the interactions is given. In general differences in the particle numbers are found to be correlated to the proton-air total

TABLE I. – *Predicted number of particles per square meter and year in the energy range of* 1 *to* 10 TeV *for the eight different models.*

	hadrons	e/γ's		hadrons	e/γ's
VENUS	5498	618	DPMJET	4143	554
QGSJET 98	5015	638	SIBYLL 2.1	5311	730
SIBYLL 1.6	7335	1084	NEXUS	4948	625
HDPM	8648	995	QGSJET 01	4439	511

cross-sections used in the respective simulations [4]. For primary helium and iron nuclei the differences of the models are of the same order as for primary protons. Considering heavier primaries no significant differences could be observed for the investigated observables which would reveal the different handling of the nucleus-nucleus interactions.

The spectra observed at the Pamir experiment stem mainly from primary protons. This is demonstrated in fig. 2 where the contributions of the different primaries to the total flux of electromagnetic particles is shown. The contribution of heavy primaries is not only reduced due to the primary fluxes but also as a consequence of the faster development of showers induced by heavy particles. Primaries of larger energies do not compensate this effect due to the steeply decreasing primary spectrum. Even if there may exist a relatively large part of medium primaries (which are not simulated for present considerations) it would not change the distribution and total number of the "all simulations" distribution of the particle spectra appreciably. The relevant primary energy range for the shower particles is around 10^{14}eV in case of protons, *i.e.* the chosen range of simulations is sufficient. Figure 3 compares the contributions to the total flux for the two versions of QGSJET showing that the expected differences are occur at all primaries.

The present simulations exhibit a basic sensitivity of emulsion chamber experiments placed in high altitudes to current models of hadronic interactions. Uncertainties due to the indetermination of the primary proton and helium fluxes are quoted to be smaller than 20% [12] for direct measurements at 100 TeV. The larger uncertainties for the heavier primaries, which determines the uncertainty of the all-particle cosmic-ray flux at these energies, are negligible at our analysis because of the small contribution of heavy primaries to the investigated secondary particle spectra (see fig. 2). Uncertainties due to reconstruction procedures will be discussed in the following sections.

3. – Detector simulations

High-sensitivity X-ray films have been used in Pamir (type Pamir RT-6M) and other emulsion experiments to determine the energy of electron-photon shower spots by means of a photometric method. In order to establish a characteristic curve of the X-ray films, the Pamir Collaboration [3] exposes the materials to a 650 MeV extracted electron beam covering a range of electron densities of 10^5–10^9 electrons/cm^2. For a homogeneous beam the optical density D has been defined as $D = -\log_{10}(I/I_0)$, where I is the intensity of light passing through the irradiated part of the film and I_0 the intensity of light passing through the unirradiated part. Assuming that the shower spots are nearly axially symmetrical for the center of the spot, the integral optical density is defined as

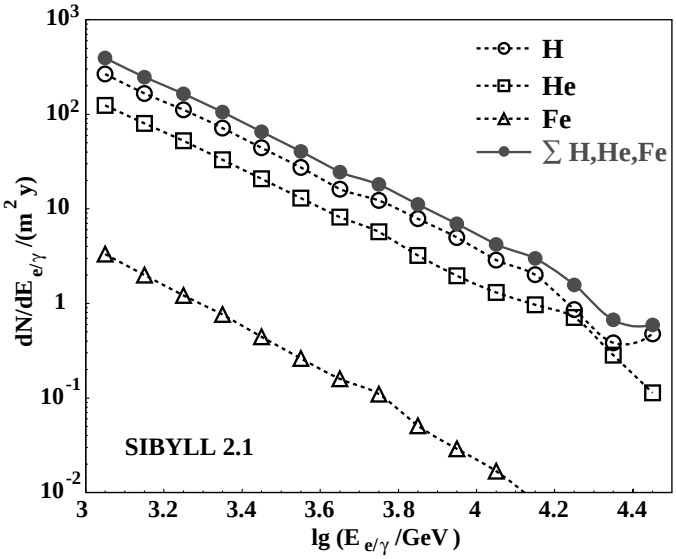

Fig. 2. – Contributions of different primary nuclei to the expected electromagnetic particle spectrum for the Pamir observation level in case of the SIBYLL 2.1 model.

$D(E_\gamma, t, r < R) = -\log_{10} \dfrac{\int_0^{2\pi} \int_0^R 10^{-D(E_\gamma,t,r)} r \mathrm{d}r \mathrm{d}\phi}{\pi R^2}$, where E_γ is the energy of the incident photon, t the depth in cascade units (c.u.), and R the radius of the diaphragm. Integral optical densities are used in emulsion experiments for the determination of energy.

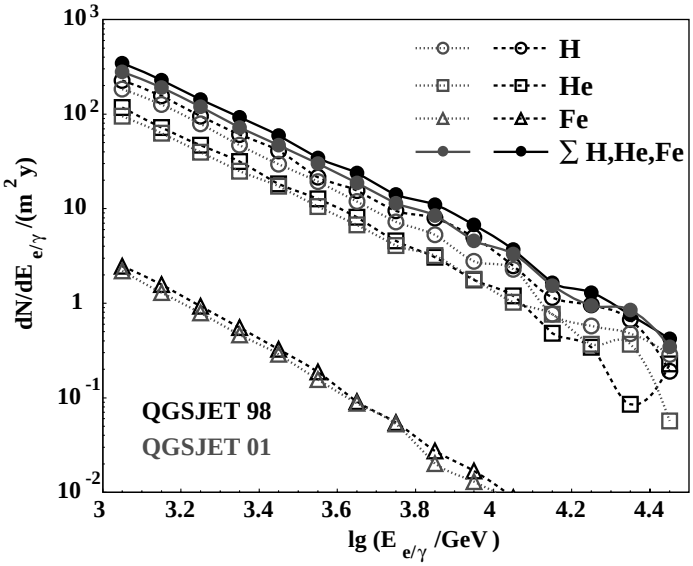

Fig. 3. – Same as fig. 2 but for the models QGSJET 98 and QGSJET 01 in comparison.

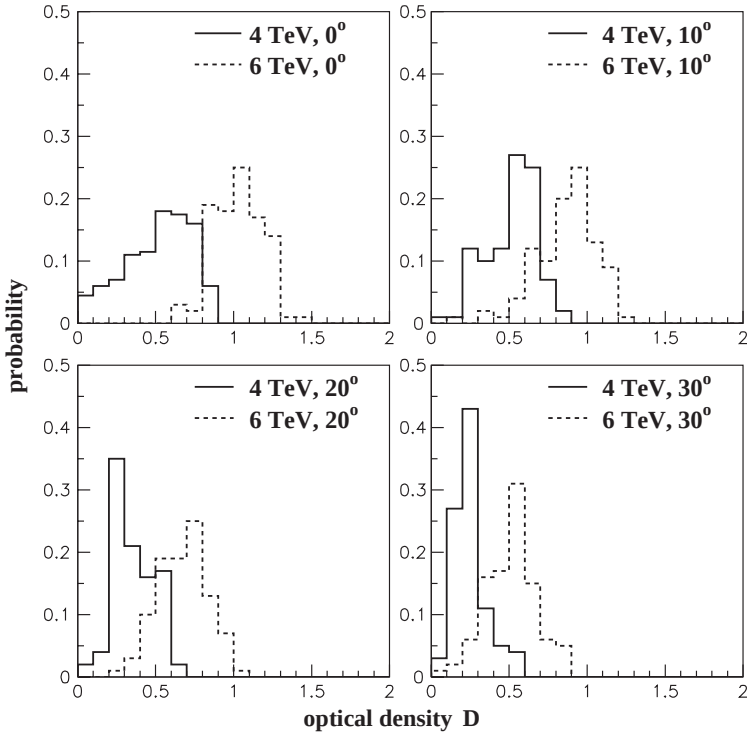

Fig. 4. – Probability distributions of the optical density of primary gamma-rays for various energies and angles of incidence.

In order to determine the optical density $D(E_\gamma, t, r)$, the form $D = D_\infty\,(1 - \exp[-\omega_0 s\rho])$ is used, where ρ is the electron density and D_∞, ω_0, and s are parameters characterizing the film type. The Pamir calorimeter has been constructed in such a way that X-ray films are positioned at the depth of 8–12 c.u., where the cascades initiated by gamma quanta of energy 4 TeV to 100 TeV reach their maxima.

For the electromagnetic particles entering the detector, detailed simulations of the detector response have been performed using the GEANT simulation tool package [14]. GEANT allows to include the geometry of the XEC-detector easily. Simulating the X-ray film the distributions of electrons with $E_\mathrm{e} \geq 1.5$ MeV in one layer, the so-called "working layer" at the depth of 10 c.u., and in bins of $10 \times 10\,\mu\mathrm{m}^2$ are considered.

The optical densities are calculated by means of the above formulas with $D_\infty = 4.0$, $\omega_0 = 1$, and $s = 3.25$ corresponding to the Pamir film material RT-6 M [15]. Figure 4 shows distributions of the optical densities D with $R = 50\,\mu$m for different primary energies and angles of incidence. These distributions show that there are large effects of fluctuations and of the zenith angle of the particle for the reconstructed densities. For primary energies from 2 to 100 TeV and for four different angles of incidence (0°, 10°, 20°, 30°) at least 100 particles have been simulated. Hence fluctuations of the densities at fixed energies and fixed angle of incidence are taken into account with high statistical accuracy in this detector simulation.

As a first approximation we adopt Gauss functions to these distributions to get a mean value and a standard deviation of the optical densities for each energy and angle of

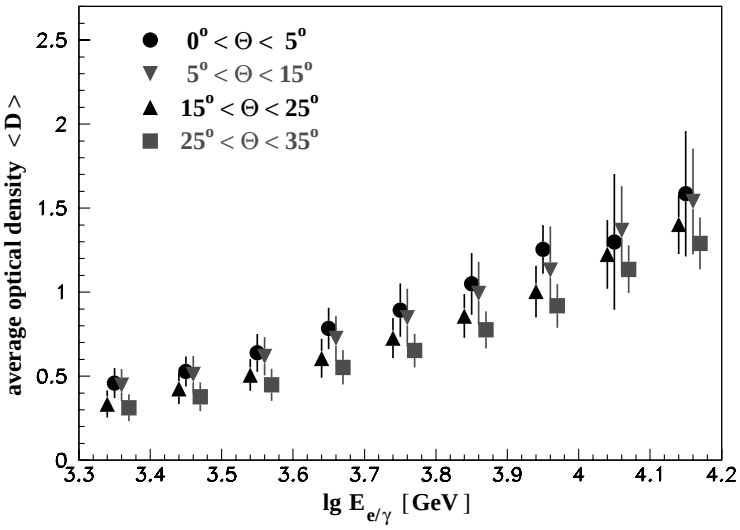

Fig. 5. – Dependence of the simulated optical density on the particle energy and angle of incidence. The error bars represent the standard deviations of the distributions.

incidence. The results have been subsequently parameterized. Hence the optical density can be calculated for each e.m. particle (of the CORSIKA simulations) with given energy and angle of incidence by interpolating the obtained distributions [16]. These procedures account for the response of the detector, including its fluctuations, and for the efficiency and threshold effects of the Pamir experiment. Figure 5 shows the resulting variation of the optical density with energy for the e/γ-particles taken from the present CORSIKA simulations.

We restrict the simulations to electromagnetic particles since the simulation of the detector response of the hadrons would require considerably more effort. Different from the electromagnetic part where electrons and gamma-rays lead to similar responses, different kinds of hadrons would have to be simulated and parameterized separately with larger statistical accuracy due to larger intrinsic fluctuations. Additionally the computing time would be much larger because the working layers for hadrons are deeper in the detector.

4. – Optical density spectra

Figure 6 shows a measured optical density distribution [17] compared to simulated distributions (QGSJET 98) including the detector response as described above. The fluxes of the simulations take into account the values of the chemical composition and spectral slopes, as given in ref. [12]. They are normalized to the exposure time of the measurement (ST = 11.5 m^2year). The strong change of the form when going from the energy spectrum to the optical density spectrum of the electromagnetic particles as a consequence of the large fluctuations in the observables is remarkable, especially at the threshold region of $D \approx 0.5$. Comparison with the data shows a good agreement in the slope of the spectrum and in the total number of particles. Even the threshold effects (the detection threshold is around 4 TeV, but with large fluctuations [16]) seem to be reproduced in a fair way. While there is a good agreement in the total number of

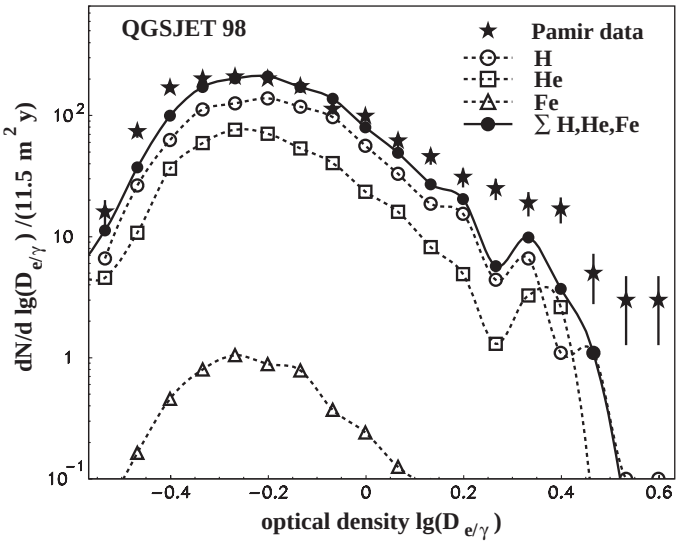

Fig. 6. – Measured optical density spectrum (ST = 11.5 m^2y) of single particles in the working layer (12 c.u.) of the Pamir experiment ($N_{e/\gamma}$ = 1469) [17] compared to spectra simulated with QGSJET 98 for different primaries and the sum. The simulations are normalized to the exposure time of the measurement.

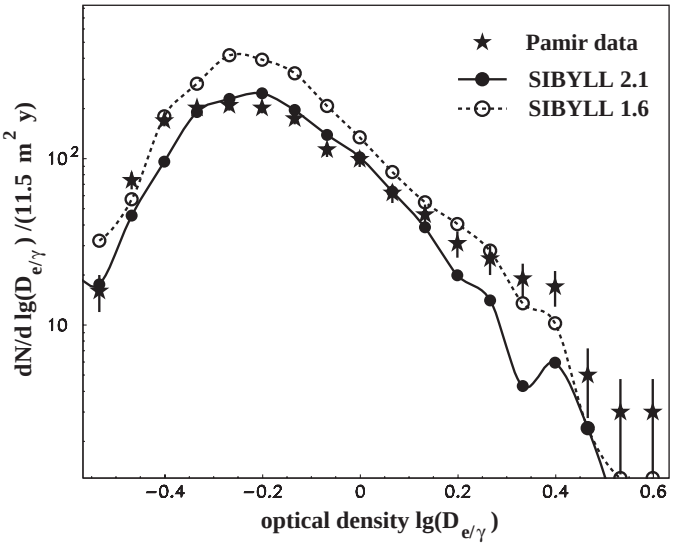

Fig. 7. – Measured optical density spectrum (ST = 11.5 m^2y) of single particles in the working layer (12 c.u.) of the Pamir experiment ($N_{e/\gamma}$ = 1469) compared to the total spectra simulated with two versions of SIBYLL. The simulations are normalized to the exposure time of the measurement.

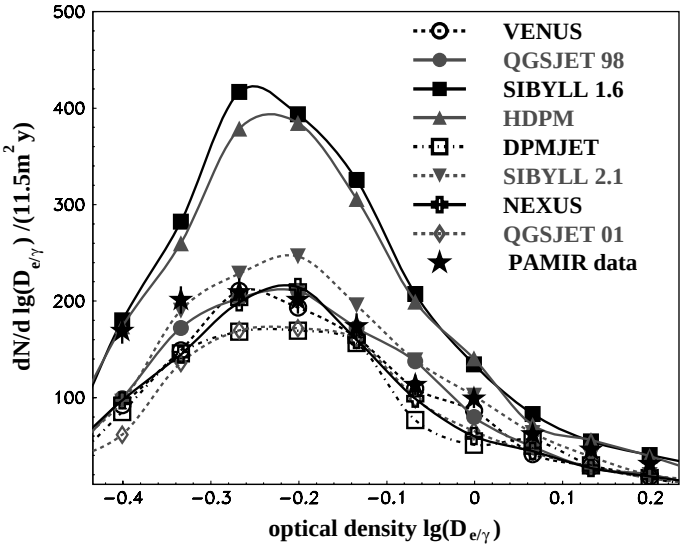

Fig. 8. – Comparison of the optical density spectrum predicted by different high-energy interaction models to the measurements. The simulated spectra are normalized to the exposure time of the measurement.

particles, there are some differences at very small optical densities (low energies). The simulation procedure only takes particles with an incident energy of > 2 TeV into account. But following calculations using the GEANT code there are some particles with lower energies which may fluctuate to optical densities larger than 0.2, which is the threshold for a "visible" spot. This would lead to an enhancement of the simulated density spectrum at low values. Furtheron the simulations do not include the probability of hadrons interacting in the upper absorber layers faking electromagnetic particles, preferentially with lower optical densities. On the other hand, the "scanning" efficiency is smaller than 100% for weak spots, *i.e.* some single particles are not identified by the processing of the emulsion films. When comparing optical density distributions for different films and years an additional uncertainty of ca. 20–30 % for the first three data points have been revealed [18]. Deviations between simulations and measurements of large optical densities (large energies) arise from the limitation of the simulations at high primary energies. The negligible contribution of particles originating from primary iron nuclei as well as the remarkably small differences for the spectral form of different primaries should be noted. For the central region of the density distribution the QGSJET 98 simulations match the data quite satisfactorily (fig. 6).

Figure 7 compares the calculated spectra for both versions of the SIBYLL model with the data. Whereas the more recent version SIBYLL 2.1 reproduces the data fairly well, the previous SIBYLL 1.6 version leads to too many particles (by about a factor of 2). This disagreement cannot be explained by statistical or systematic uncertainties. The flux and chemical composition used for the simulations may be affected by uncertainties of approximately 20% in the relevant primary energy region and the contribution of hadronic particles which produce measurable spots at the working layer of the emulsion experiment has an uncertainty of max.+20%. The latter effect is not included in the simulations, it could increase the total number of the simulated spectra, increasing the

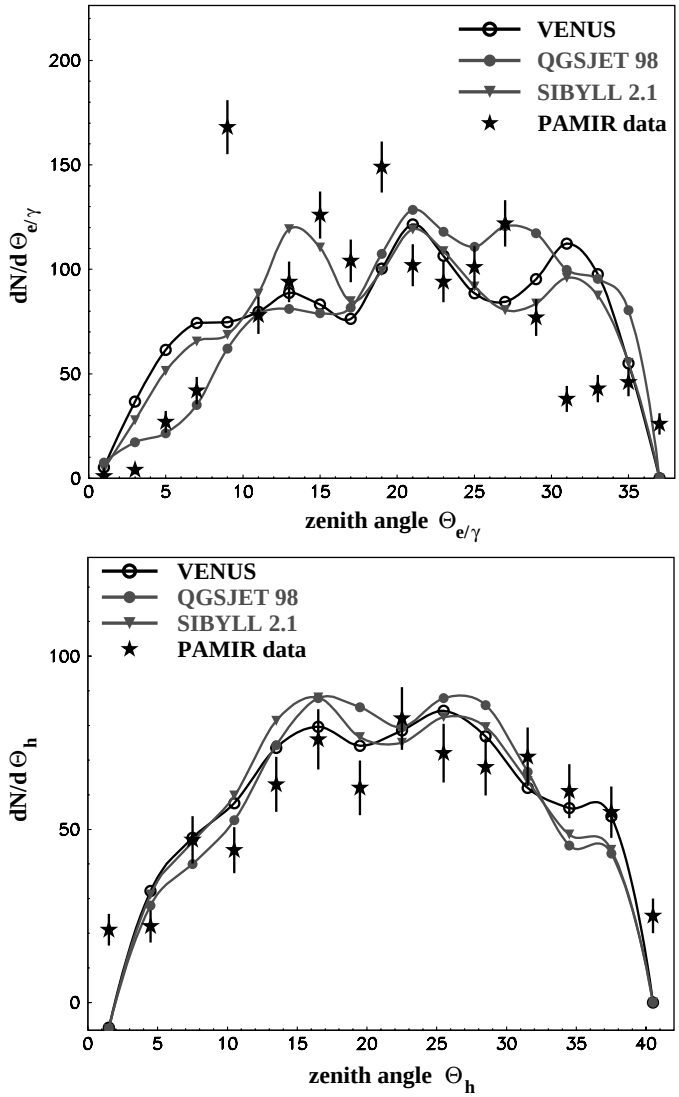

Fig. 9. – The angular distribution of single electromagnetic particles (ST = 11.5 m^2y, $D_{e,\gamma} > 0.2$) and hadronic particles (ST = 24 m^2y, $E > 7$ TeV) measured by the Pamir experiment compared to simulated distributions from different models. The simulated distributions are normalized to the measured total number $N_{e,\gamma}$ and N_h, respectively.

disagreement with the SIBYLL 1.6 model.

In fig. 8 the predictions of all eight considered interaction models are compared at the measurements for the medium region of the optical density shown at a linear scale. The differences in particle numbers as revealed in fig. 1 are still visible after including the detector response. Obviously, the SIBYLL (version 1.6) and HDPM models predict the largest numbers. Their particle fluxes are far off the measurements. SIBYLL 2.1 overestimates the electromagnetic particles above TeV energies as compared to the ob-

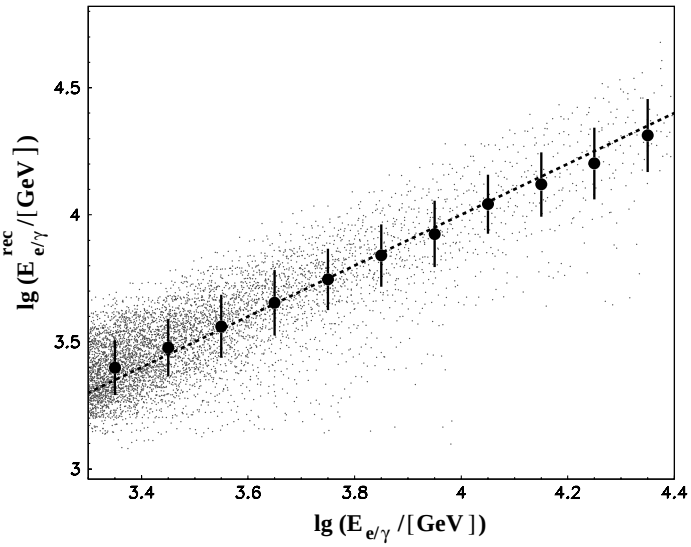

Fig. 10. – Comparison of the reconstructed energy with the true energy of all electromagnetic particles. Each small dot represents a single particle, the big dots are the reconstructed mean energy with its standard deviation at each bin. For guiding the eyes a line for $E^{\mathrm{rec}} = E^{\mathrm{true}}$ is plotted.

servations at Pamir. The models VENUS and QGSJET 98 and neXus are found to have differences smaller than the uncertainties and the predictions are in agreement with the measurements. The DPMJET and QGSJET 01 models tend to underestimate the total number of particles.

5. – Angular distributions

An additional observable of emulsion experiments is the zenith distances of single electromagnetic and hadronic particles. The special set-up of such experiments with thin lead absorbers intersected by sensitive films achieves an excellent angular resolution for the single particles [3]. Hence we can compare the angular distributions generated with CORSIKA to the measured distributions. In case of electromagnetic particles an optical density of larger than 0.2 is required.

In the upper panel of fig. 9 the comparison between the measured and simulated angular distributions of electromagnetic particles is shown. Results from different primaries and different high-energy interaction models are hardly distinguishable. This is also true for the hadronic angular distributions (fig. 9, lower panel). Here the intrinsic fluctuations are smaller than in the case of electromagnetic particles due to missing families. For such families, a large number of particles have equal angle of incidence. The shown distributions reflect the zenith-angle distribution of the cosmic-ray primaries contributing to the spectra, showing that most of the measured particles are produced in the extreme forward direction.

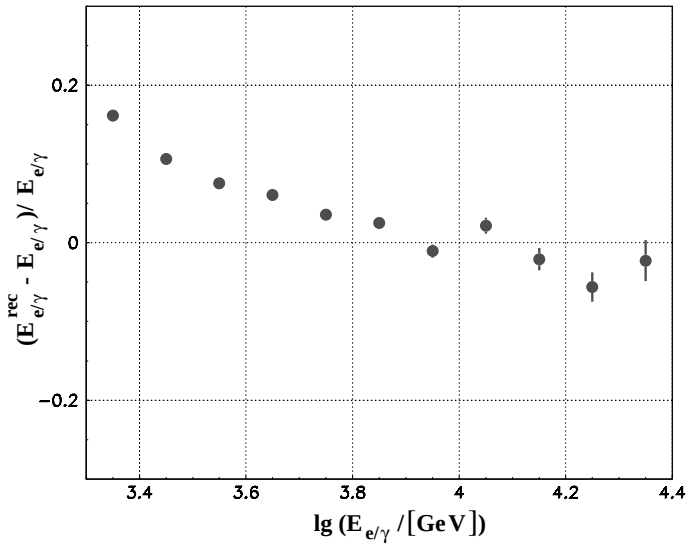

Fig. 11. – The energy resolution of the reconstruction procedures of the Pamir experiment for secondary electromagnetic shower particles. The error bars represent the statistical accuracy.

6. – Energy reconstruction

Via the simulation of the optical density the primary energy of the single electromagnetic particles can be reconstructed, using the reconstruction procedures of the Pamir experiment [19,18]. For each particle the energy reconstruction uses the calculated optical density for the $r = 50\,\mu$m diaphragm and the zenith angle of the particle. Figures 10 and 11 show the quality of the energy reconstruction achieved by this procedure for all simulated particles with an integral optical density larger than 0.2. In spite of the large fluctuations the average reconstruction quality is quite good with a relative error of less than 20% and nearly independent of the species of the particle (gamma or electron) but the resolution is energy dependent. Near threshold the reconstructed energy appears to be slightly larger than the true one. At energies above 10 TeV a tendency for underestimating the energy is indicated.

Figure 12 shows the integral energy spectra reconstructed from the Pamir data for different interaction models including the detector response and the reconstruction procedures. The detection efficiency affects the spectra up to 5 TeV. For energies above 10 TeV the limited Monte Carlo statistics for ultra-high primary energies are affecting the spectra. But the general features of the different interaction models still persist: the expected slopes are not very different but the total flux varies for the different interaction models more than within the uncertainties of the measurements. Nevertheless the reconstructed energy spectra reproduce the initial spectra (*i.e.* those obtained by pure air-shower simulation ignoring detector response and reconstruction efficiencies, see fig. 1) surprisingly well in the energy region between 5 and 10 TeV. The gross features of the CORSIKA simulations still persist in spite of the large fluctuations and threshold effects of the reconstruction. Therefore the slope and flux values of the spectra can be compared with the measured integral energy spectrum presented by the Pamir collaboration [20]: $I(>E) = (1.63 \pm 0.13) \cdot 10^{-6} \cdot (E/5\,\mathrm{TeV})^{-1.93\pm0.12}$ $(\mathrm{m}^{-2}\mathrm{s}^{-1}\mathrm{sr}^{-1})$. For

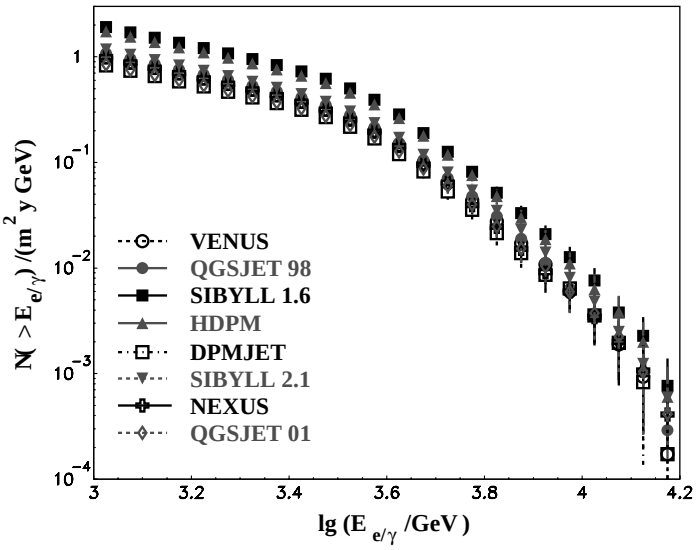

Fig. 12. – Energy spectra of secondary electromagnetic secondary shower particles after taking into account the detector response and reconstruction procedures as expected for the Pamir observation level for different interaction models. The spectra are displayed in integral form and normalized to an exposure time of ST = 1 m^{2}year.

comparison we adopt a power law function $I(>E) = A \cdot 10^{-6} \cdot (E/5\,\mathrm{TeV})^{-\beta}$ for the simulated integral spectra and calculated the slope parameter β and the flux value A at 5 TeV for each model. The slope parameters vary between 1.9 and 2.5 for the different models but all models reproduce the slope of the measured spectrum within their statistical accuracies, but the flux for electromagnetic particles above 5 TeV predicted by some of the models (SIBYLL 1.6 $A = 3.9 \pm 0.4$, HDPM $A = 3.6 \pm 0.4$) deviates by a factor exceeding the uncertainties. The hadronic interaction models VENUS ($A = 2.0 \pm 0.4$), NEXUS ($A = 2.0 \pm 0.4$), and QGSJET 98 ($A = 2.2 \pm 0.4$) show the best agreement with the measurements, also after the full reconstruction procedures, which includes the flux generation according to [12], a full simulation of the air-shower development with CORSIKA, the detailed simulation of the detector response, and the reconstruction of the particle energies with help of the original Pamir algorithms.

7. – e/γ-families

In addition to the single-particle spectra, high-altitude emulsion experiments measure also groups of several numbers of spots originating from the same air-shower, the so-called e/γ-families. The families result from primary energies in the PeV region, and the flux and characteristics of such families are used to reconstruct the energy spectrum and chemical composition of the primary cosmic rays in this range [3] where the energy spectrum shows a kink ("knee") in the slope. Main characteristics of such families are the energy sum of the family members, the mean radius R, and the mean value ER of the product of energy and radius.

In the present analyses we use the simulation procedures described above for an estimate of the mass sensitivity and for reproduction of the mean characteristics of families

TABLE II. – *Average characteristics mean radius* $\langle R\rangle$ *and mean value of energy weighted radius* $\langle ER\rangle$ *of* e/γ*-families in the range of* $\Sigma E_{e/\gamma} = 100$–$200\,\mathrm{TeV}$. *Pure CORSIKA simulations as well as simulations including the detector response and reconstruction procedures are compared for three hadronic interaction models to the results of the Pamir experiment* [21]. *The same requirements for the family reconstruction are applied to simulations and data (see text).*

Model	Proton	He	Pamir experiment	
pure CORSIKA				
QGSJET 98	23±2	25±2	23±1	$\langle R\rangle$(mm)
	198±15	202±15	210±10	$\langle ER\rangle$(TeV · mm)
SIBYLL 2.1	26±2	32±2	23±1	$\langle R\rangle$(mm)
	219±16	279±22	210±10	$\langle ER\rangle$(TeV · mm)
HDPM	30±2	36±3	23±1	$\langle R\rangle$(mm)
	253±19	324±26	210±10	$\langle ER\rangle$(TeV · mm)
reconstructed				
QGSJET 98	27±2	31±2	23±1	$\langle R\rangle$(mm)
	208±14	245±17	210±10	$\langle ER\rangle$(TeV · mm)
SIBYLL 2.1	28±2	35±3	23±1	$\langle R\rangle$(mm)
	226±16	292±21	210±10	$\langle ER\rangle$(TeV · mm)
HDPM	31±2	39±3	23±1	$\langle R\rangle$(mm)
	252±17	326±24	210±10	$\langle ER\rangle$(TeV · mm)

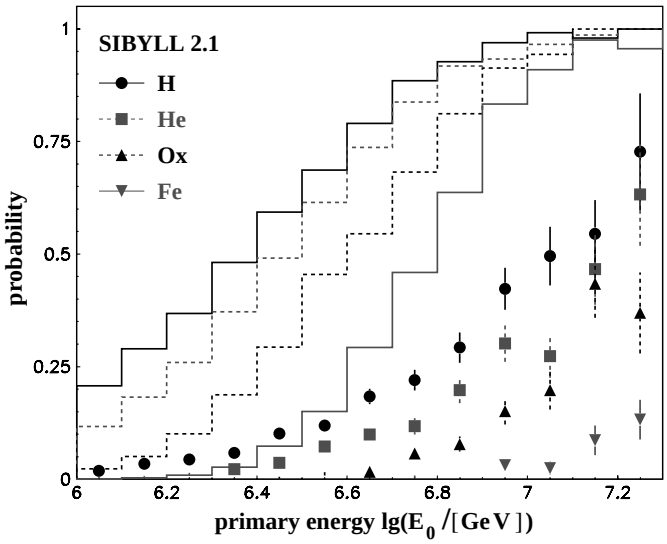

Fig. 13. – Primary energy dependence for the probability to produce an e/γ-family in case of pure air-shower simulations (lines) and including the detector response (markers) for different primary species.

as recorded by the Pamir collaboration [21]. The possible sensitivity to various interaction models will be discussed. For that purpose we extended for some models the statistical accuracy of CORSIKA simulations for the energy region around and above the knee. We generate for primary protons, helium, oxygen and iron nuclei and for the models HDPM, QGSJET 98, and SIBYLL 2.1 20000 primaries each in the energy range 10^{15} eV–$3.16 \cdot 10^{16}$ eV (slope $\gamma = -2.75$) and put the same procedures to the secondary particles as described above, *i.e.* the full detector simulation and energy reconstruction.

In ref. [21] a family is defined as a group of more than 3 particles with reconstructed energy of > 4 TeV in a circle of less than 150 mm radius in the working layer of the e/γ-block of Pamir, originating from the same shower. For the simulations we require the same conditions for a family, but we distinguish between families selected after the shower development with the energy cut applied to the true energy, and families selected after simulating the detector response with the energy cut applied to the reconstructed energy of the particles.

Figure 13 shows for the case of the SIBYLL model the energy dependence of the probability to produce a family by the various primaries. The reduction of the detection efficiencies when taking into account the threshold effects of the reconstruction is obvious. These efficiencies scale with the absolute number of electromagnetic particles (see fig. 1) predicted by the models. Thus QGSJET 98 predicts lower and HDPM higher probabilities to produce families. But all model predictions agree in the contribution of various primaries to the number of measured families, *i.e.* that they are mainly produced by light primaries. Thus, the measured samples of families consist mainly of protons (light primaries), disadvantageous for the reconstruction of the cosmic-ray mass composition, though the effect is less pronounced than in case of single particles. But such a selection gives the chance to study properties of the proton interactions with atmospheric nuclei.

In table II the family characteristics: mean radius and energy weighted mean radius of the simulated events are compared with results of the Pamir experiment [21]. In the simulations an increase of both parameters is observed with mass and with the total particle multiplicity produced by the models. Compared with data the values for nuclei heavier than helium are so large that they evidently disagree with the experimental results. This is true although the statistical accuracy of the simulated families is poor. This holds also for the data sample incorporating the detection probabilities in fig. 13. Only the QGSJET 98 model results in values close to those of the data. Again SIBYLL 2.1 and HDPM predict too many particles and with it too large values for $\langle R \rangle$ and $\langle ER \rangle$. This tendency proves the sensitivity of the measurements to the interaction models even at larger primary energies via family parameters. The fully reconstructed values for $\langle R \rangle$, *i.e.* the mean distance between high-energy gamma-rays in the EAS, are too large even for the QGSJET 98 model. It was found that $\langle R \rangle$ depends stronger on the incident primary energy spectrum than $\langle ER \rangle$. Considering the values of $\langle ER \rangle$, the predicted results for QGSJET 98 support a heavier primary composition if only the air-shower development is simulated ignoring the detector response. The latter point should be taken into account if these family parameters are used for estimates of the chemical composition of primary cosmic rays.

8. – Conclusions

Experiments located at high mountain altitudes like the Pamir experiment register high-energy hadrons, e/γ-rays, and e/γ-rays families. The measurements cover a wide range of primary energies: from tens of TeV for single particles up to hundreds of PeV

for the e/γ families. We could show that the observables of these emulsion experiments have only a small contribution of events induced by primary iron nuclei within the whole energy range. The high-energy particle detection threshold naturally selects and enhances light primaries in the measured spectra of e/γ's and hadrons, and also of e/γ-families.

The typical observables of emulsion experiments at high mountains are sufficiently sensitive for testing current high-energy hadronic interaction models. Though there are uncertainties in the knowledge of the primary spectrum and chemical composition certain models could be excluded. The experimental results prove to be sensitive to the particular theoretical approaches for the interaction of high-energy light nuclei with air molecules. The investigated particles stem mainly from primary cosmic rays of energies below 1 PeV and have been produced in extreme forward direction. This explains the special suitability of these measurements for tests of high-energy hadronic interaction models: The measured particles carry information complementary to the data of accelerator experiments where the extreme forward direction is not covered by the detectors.

We found that the SIBYLL 1.6 and HDPM models are unable to reproduce the data. The SIBYLL 1.6 and the HDPM model produce generally too many high-energy particles to match the measured distributions. Particularly the flux of high-energy electromagnetic particles is overestimated, especially in the well-reproduced range of the optical density $0.5 < D < 1.2$. We conclude that either the proton-air cross-section is too low or the implemented inelasticity coefficient is too small for these models. This result is confirmed by investigations of the characteristics of e/γ-families. In contrast, the models QGSJET 98, neXus, and VENUS based on the Gribov-Regge theory can reproduce the data satisfactorily. The DPMJET, and QGSJET 01 models tend to underestimate and the SIBYLL 2.1 model tends to overestimate the measured flux. The exclusion of predictions using the SIBYLL 1.6 model is in agreement with model tests with air-shower data measured at sea-level by the KASCADE experiment [22, 23].

It should be noted that the sensitivity to model tests is achieved only with detailed detector simulations accounting for the large intrinsic fluctuations and threshold effects. The observed differences between the model predictions confirm the sensitivity of the Pamir experiment to hadronic interaction features. This sensitivity may be further enhanced by taking into account also the correlations between the different observables, *e.g.*, the hadronic and electromagnetic information of the Pamir experiment on single events. This study requires a refinement of detailed detector simulations of the hadronic response of the detector installation.

* * *

We would like to thank D. Heck for embedding the considered models in the CORSIKA code and J. Malinowski and A. Iwan for valuable discussions concerning the reconstruction procedures at Pamir. We thank S. Ostapchenko for useful discussions on the physics of the models and H. Rebel and G. Schatz for comments on the manuscript.

REFERENCES

[1] Klages H. O. *et al.* (KASCADE Collaboration), *Nucl. Phys. B (Proc. Suppl.)*, **52B** (1997) 92.
[2] Antoni T. *et al.* (KASCADE Collaboration), *Astropart. Phys.*, **16** (2002) 245.
[3] Baradzei L. T. *et al.* (Chacaltaya and Pamir Collaboration), *Nucl. Phys. B*, **370** (1992) 365.

[4] Heck D. *et al.*, FZKA report 6019, Forschungszentrum Karlsruhe (1998).
[5] Werner K., *Phys. Rep.*, **232** (1993) 87.
[6] Kalmykov N. N., Ostapchenko S. S. and Pavlov A. I., *Nucl. Phys. B (Proc. Suppl.)*, **52B** (1997) 17.
[7] Engel J. *et al.*, *Phys. Rev. D*, **46** (1992) 5013.
[8] Ranft J., *Phys. Rev. D*, **51** (1995) 64.
[9] Engel R. *et al.*, *Proceedings of the 26th International Cosmic Ray Conference (ICRC), Salt Lake City*, Vol. **1** (1999) 415.
[10] Ostapchenko S. S., private communication (2001).
[11] Drescher H. J. *et al.*, *Phys. Rep.*, **350** (2001) 93.
[12] Wiebel-Sooth B. *et al.*, *Astron. Astrophys.*, **330** (1998) 389.
[13] Nelson W. R., Hirayama H. and Rogers D. W. O., SLAC report 265, Stanford Linear Accelerator Center (1985).
[14] Brun R. *et al.*, CERN Cern long writeup: GEANT vers. 3.21 (1993).
[15] Haungs A. and Kempa J., *Proceedings of the 25th International Cosmic Ray Conference (ICRC), Durban*, Vol. **6** (1997) 101.
[16] Haungs A., Kempa J. and Malinowski J., *Proceedings of the 26th International Cosmic Ray Conference (ICRC), Salt Lake City*, Vol. **1** (1999) 123.
[17] Bialobrzeska H. *et al.*, *Nucl. Phys. B (Proc. Suppl.)*, **75A** (1999) 162.
[18] Haungs A., Kempa J. and Malinowski J., *Nucl. Phys. B (Proc. Suppl.)*, **97** (2001) 134.
[19] Roganova T. and Ivanenko I. P., private communication (1987).
[20] Bialawska H. *et al.*, *Bull. Soc. Sci. Lett. Lodz*, **23** (2001) 109.
[21] Borisov A. *et al.*, *Proceedings of the 26th International Cosmic Ray Conference (ICRC), Salt Lake City*, Vol. **1** (1999) 84.
[22] Antoni T. *et al.* (KASCADE Collaboration), *J. Phys. G*, **25** (1999) 2161.
[23] Antoni T. *et al.* (KASCADE Collaboration), *J. Phys. G*, **27** (2001) 1785.